

The tidal stripping of satellites

J. I. Read ^{1*} M. I. Wilkinson ¹ N. W. Evans ¹ G. Gilmore ¹ & Jan T. Kley ²

¹*Institute of Astronomy, Cambridge University, Madingley Road, Cambridge, CB3 0HA, England*

²*Institute for Astronomy, University of Hawaii, 2680 Woodlawn Drive, Honolulu, HI 96822*

2 December 2024

ABSTRACT

We present an improved analytic calculation for the tidal radius of satellites and test our results against N-body simulations.

The tidal radius in general depends upon four factors: the potential of the host galaxy, the potential of the satellite, the orbit of the satellite and, which is new to this paper, *the orbit of the star within the satellite*. We demonstrate that this last point is critical and suggest using *three tidal radii* to cover the range of orbits of stars within the satellite. In this way we show explicitly that prograde star orbits will be more easily stripped than radial orbits; while radial orbits are more easily stripped than retrograde ones. This result has previously been established by several authors numerically, but can now be understood analytically.

Over short times ($\lesssim 1 - 2$ Gyrs ~ 1 satellite orbit), we find excellent agreement between our analytic and numerical models. Over longer times, star orbits within the satellite are transformed by the tidal field of the host galaxy. In a Hubble time, this causes a convergence of the three limiting tidal radii towards the prograde stripping radius. We predict that, beyond the prograde stripping radius, the velocity dispersion is tangentially anisotropic.

Key words: galaxies: dwarf, galaxies: star clusters, galaxies: kinematics and dynamics

1 INTRODUCTION

The tidal radius is the radius at which a star within a satellite becomes unbound or stripped and becomes bound instead to the host galaxy about which the satellite orbits. The problem of calculating the tidal radius of satellites has a long history which dates back to von Hoerner (1957) who analysed the problem in the context of globular clusters around the Milky Way.

It is a problem with a very wide scope of application, from understanding the sharp edge observed in some nearby globular clusters (King 1962), to semi-analytic modelling of galaxy formation, where interactions and mergers play a vital role in our current hierarchical formation paradigm (Taffoni et al. 2003). It is a problem which has also experienced a renaissance with the advent of so-called ‘near-field cosmology’. Our current cosmological models are beginning to give precise predictions for the distribution, abundance and morphology of satellite galaxies (Moore et al. 1999), while data from the nearest satellites within the Local Group can provide excellent constraints on these theories (Mateo 1998). Understanding in detail the effects of a tidal field on the stars and dark matter particles within a satellite are central to these modern branches of astrophysics.

In this paper, we revisit this old problem and present an improved analytic calculation for the tidal radius of satellites. It has been understood, at least numerically, for some time that the tidal radius in general depends upon four factors: the potential of the host galaxy, the potential of the satellite, the orbit of the satellite and, *the orbit of the star within the satellite*. To our knowledge, however, only the first three factors have been addressed in analytic calculations previously (see e.g. von Hoerner 1957 and King 1962). Here, we present an analytic calculation which includes the effect of the orbit of the star too.

That the orbit of the star is important has been noted several times in the past. Toomre & Toomre (1972) found numerically that prograde orbits are more easily stripped than retrograde orbits, while Keenan & Innanen (1975) showed that both radial and prograde orbits are more easily stripped than retrograde orbits. More recently, Kazantzidis et al. (2004) and Kravtsov et al. (2004) have found that the satellites in their simulations show tangential velocity anisotropy near the tidal radius and that radially biased velocity distributions are more rapidly stripped. Similar results have been observed in globular cluster and star cluster simulations (Takahashi et al. 1997, Giersz & Heggie 1997 and Baumgardt & Makino 2003). All of these numerical results point to the fact that the orbits of stars play an important role in determining the tidal radius for the satellite. In this

* Email: jir22@ast.cam.ac.uk

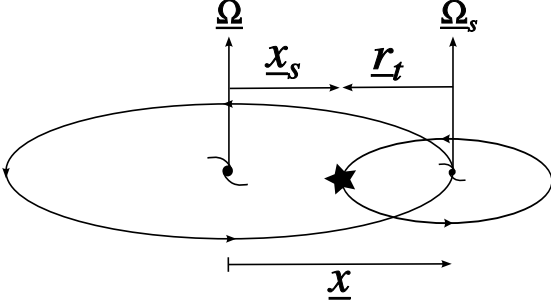


Figure 1. A schematic diagram of the analytic set-up. The satellite and the star within the satellite both orbit in the x - y plane with angular velocities $\underline{\Omega}$ and $\underline{\Omega}_s$ respectively. We consider the problem from a frame centred on the host galaxy rotating with angular velocity $\underline{\Omega}(t)$. In this frame the centre of mass of the satellite is stationary. In this diagram, the star (marked by the black star) is on a prograde orbit; see text for further details.

paper, we shed some analytic insight on these numerical observations.

This paper is organised as follows: in section 2 we present our calculation for the tidal radius of spherical systems. We include the effect of the orbit of the star within the satellite by considering three limiting cases of interest: prograde and retrograde circular star orbits, and pure radial star orbits. In section 3, we then compare our analytic formulae with detailed N-body simulations of tidal stripping and show that they provide an excellent fit to the simulation data. Finally, in section 4, we present our conclusions.

2 AN ANALYTIC CALCULATION OF THE TIDAL RADIUS

A schematic diagram of the analytic set-up is shown in Figure 1. We analyse the problem from a frame rotating with angular velocity, $\underline{\Omega}(t)$, centred on the host galaxy. We can choose $\underline{\Omega}(t)$ such that the centre of mass of the satellite will always be stationary in this frame. Using Lagrangian methods as in Binney & Tremaine (1987), the equation of motion for the centre of mass of the satellite in this frame is given by:

$$\ddot{\underline{x}} + \dot{\underline{\Omega}} \wedge \underline{x} + 2\underline{\Omega} \wedge \dot{\underline{x}} + \underline{\Omega} \wedge (\underline{\Omega} \wedge \underline{x}) + \nabla V_g(\underline{x}) = 0 \quad (1)$$

where \underline{x} is the vector distance joining the centre of mass of the satellite to that of the host galaxy, and $\nabla V_g(\underline{x})$ is the force per unit mass due to the host galaxy potential, $V_g(\underline{x})$, on the centre of mass of the satellite.

In the same frame as above, the equation of motion for a star at an instantaneous distance, \underline{x}_s , from the host galaxy is given by:

$$\ddot{\underline{x}}_s + \dot{\underline{\Omega}} \wedge \underline{x}_s + 2\underline{\Omega} \wedge \dot{\underline{x}}_s + \underline{\Omega} \wedge (\underline{\Omega} \wedge \underline{x}_s) + \nabla V_g(\underline{x}_s) + \nabla V_s(\underline{r}_t) = 0 \quad (2)$$

where $\nabla V_s(\underline{r}_t)$ is the force on the star due to the satellite and $\underline{r}_t = \underline{x}_s - \underline{x}$ is the instantaneous tidal radius of the star. Note that from here on we will assume in this calculation that the star is at its instantaneous tidal radius, $\underline{r} = \underline{r}_t$.

For the special case of stars on pure circular or pure radial orbits (two limiting extremes of interest), we may write:

$$\dot{\underline{x}}_s = \dot{\underline{x}} + \underline{\Omega}_s \wedge \underline{r}_t \quad (3)$$

where $\underline{\Omega}_s$ is the angular velocity of the star about the centre of mass of the satellite. Equation (3) is valid for circular orbits because in this case the space velocity of the star is due only to the velocity of the satellite galaxy plus that due to its rotation, $\underline{\Omega}_s$. It is also valid for pure radial orbits because in this case, not only does $\underline{\Omega}_s \rightarrow 0$, but crucially, at the apocentre of the star's orbit, the radial component of the star's space velocity about the satellite must also be zero. Since all stars on radial orbits with apocentres larger than the instantaneous tidal radius will be stripped, we may take the limiting case where radial star orbits at the tidal radius are at apocentre.

Equating equations (1) and (2), substituting for equation (3), and using the fact that at the tidal radius, $\ddot{\underline{x}}_s - \ddot{\underline{x}} = 0$, we obtain the following equation for r_t :

$$\underline{F}_f + \underline{F} = 0 \quad (4)$$

where

$$\underline{F} = \nabla V_g(\underline{x}) - \nabla V_g(\underline{x}_s) - \nabla V_s(\underline{r}_t) \quad (5)$$

$$\underline{F}_f = \dot{\underline{\Omega}} \wedge \underline{r}_t + \underline{\Omega} \wedge (\underline{\Omega} \wedge \underline{r}_t) + 2\underline{\Omega} \wedge (\underline{\Omega}_s \wedge \underline{r}_t) \quad (6)$$

Notice that the Coriolis terms, $2\underline{\Omega} \wedge \dot{\underline{x}}$, have cancelled. For the case of stars on pure radial orbits where $\underline{\Omega}_s \rightarrow 0$, all Coriolis terms disappear which is why in the original calculation by King (1962), such terms can be left out.

Equations (5) and (6) are still quite unwieldy and give a continuum of tidal radii for stars on different orbits and different alignments to the orbital plane of the satellite. We may greatly simplify things, however, by searching for the smallest tidal radii. This occurs for the co-planar orientation shown in Figure 1. By placing the star in the same orbital plane as the satellite, the star's rotational velocity then maximally adds to (prograde orbits) or subtracts from (retrograde orbits) the space velocity of the satellite about the host galaxy. Furthermore, we are interested in the phase of the star's orbit which similarly minimises the tidal radius. This is when the star is aligned along the line of centres of the host galaxy and satellite as shown in Figure 1. At this point the star is both at its closest approach to the host galaxy and at the point where its rotational velocity is of maximal effect.

Using the geometry of Figure 1 and taking just the force component along the line of centres of the host galaxy and satellite (along $\hat{\underline{x}}$), we obtain:

$$\underline{F}_f \cdot \hat{\underline{x}} + \underline{F} \cdot \hat{\underline{x}} = 0 \quad (7)$$

where

$$\underline{F} \cdot \hat{\underline{x}} = \left. \frac{dV_g}{dx} \right|_x - \left. \frac{dV_g}{dx} \right|_{|x-r_t|} + \left. \frac{dV_s}{dr} \right|_{r_t} \quad (8)$$

$$\underline{F}_f \cdot \hat{\underline{x}} = -\Omega^2 r_t - 2\Omega \Omega_s r_t \quad \text{prograde}$$

$$\underline{F}_f \cdot \hat{\underline{x}} = -\Omega^2 r_t \quad \text{radial}$$

$$\underline{F}_f \cdot \hat{\underline{x}} = -\Omega^2 r_t + 2\Omega \Omega_s r_t \quad \text{retrograde} \quad (9)$$

Notice that the terms involving $\dot{\underline{\Omega}}$ vanish in this geometry and that we have introduced the notation: $\Omega = |\underline{\Omega}|$; and similarly for the other vectors.

For the extremal cases of pure circular and pure radial orbits, we now have three tidal radii for prograde, radial and retrograde orbits. It is instructive to rearrange equation (7) to give:

$$\frac{GM_s(r_t)}{r_t^2} = \frac{GM_g(x - r_t)}{(x - r_t)^2} - \frac{GM_g(x)}{x^2} - \Omega^2 r_t \pm 2\Omega\Omega_s r_t \quad (10)$$

where $M_s(r)$ and $M_g(x)$ are the satellite and host galaxy mass distributions respectively. Two important points can be made from equation (10). First, the right hand side will be maximised for retrograde orbits and minimised for prograde orbits. Thus, we expect that prograde orbits are more easily stripped than radial orbits; while radial orbits are more easily stripped than retrograde orbits. This will be tested against numerical experiments in section 3. Secondly, if $\Omega_s = 0$ - which is the case for stars on pure radial orbits - then the tidal radius depends only on the mass within r_t , for the satellite, and x for the host galaxy. Thus we recover the familiar result that the tidal radius depends only on the mean densities of the satellite and host galaxy, but not on their mass distributions. However, this is *only true for stars on radial orbits*. Once the star orbits are taken into account and $\Omega_s(r_t)^2 = GM_s(r_t)/r_t^3 \neq 0$ then the tidal radius will depend on the mass distributions as well as the mean enclosed densities. This point is a direct and important consequence of including the effect of star orbits in the calculation of the tidal radius.

For spherical symmetry, the energy equation for the satellite may be rearranged to give:

$$J^2 = 2 \frac{(V_g(x_p) - V_g(x_a))x_a^2 x_p^2}{x_p^2 - x_a^2} \quad (11)$$

$$E = \frac{J^2}{2x_a^2} + V_g(x_a) \quad (12)$$

where J is the specific angular momentum of the satellite, E is the specific energy and x_p and x_a are the satellite pericentre and apocentre respectively. The satellite orbit is then fully specified by $x_p < x < x_a$ and we may readily obtain $\Omega(t) = J/x(t)^2$ from equation (11).

Since $\Omega = \Omega(t)$ and $x = x(t)$, for all but circular satellite orbits, the three limiting tidal radii solutions to equation (7) are a *function of time*: $r_t = r_t(t)$. Whether a time independent value for the tidal radius is appropriate in such situations is discussed further in section 3.3.

Given $V_g(x)$, $V_s(r_t)$, $x(t)$, x_p and x_a , we now have enough information to solve equation (7) for the three values of $r_t(t)$. In general, this solution must be found numerically. An analytic solution may be obtained, however, for the special case of point mass potentials for the satellite and host galaxy, in which case the satellite's orbit is Keplerian. In this case, equation (11) gives us:

$$\Omega^2 = \frac{GM_g}{x^4} \kappa \quad (13)$$

$$\kappa = \frac{2x_a x_p}{x_a + x_p} = a(1 - e^2) \quad (14)$$

where G is the gravitational constant, M_g is the mass of the host galaxy and we define here the standard Keplerian semi major axis, a , and eccentricity, e , as:

$$e = \frac{x_a - x_p}{x_a + x_p} \quad (15)$$

$$a = \frac{x_a + x_p}{2} \quad (16)$$

In fact, these definitions involve only x_a and x_p , and so hold good for any orbit in a spherical potential.

Substituting equation (13) into equation (7), using point mass potentials, and solving, we obtain:

$$r_t \simeq \left(x^4 \frac{M_s}{M_g} \kappa \right)^{1/3} \left(\frac{\sqrt{\alpha^2 + 1 + 2x/\kappa} - \alpha}{\kappa + 2x} \right)^{2/3} \quad (17)$$

where M_s and M_g are the mass of the satellite and host galaxy respectively and α is a parameter which defines the orbit of the star within the satellite in the following way:

$$\alpha = \begin{cases} 1 & \text{prograde} \\ 0 & \text{radial} \\ -1 & \text{retrograde} \end{cases} \quad (18)$$

Equation (17) gives $r_t(x)$ or since $x = x(t)$, equivalently, $r_t(t)$. As originally suggested by von Hoerner (1957) and King (1962), we may take the limiting case which gives the smallest tidal radius - namely that at pericentre; $x = x_p$. In this case, equation (17) reduces to:

$$r_t \simeq x_p \left(\frac{M_s}{M_g} \right)^{1/3} \left(\frac{1}{1+e} \right)^{1/3} \left(\frac{\sqrt{\alpha^2 + 1 + \frac{2}{1+e}} - \alpha}{1 + \frac{2}{1+e}} \right)^{2/3} \quad (19)$$

It is reassuring to note that, for the case of pure radial star orbits, $\alpha = 0$ and equation (19) reduces to the familiar King (1962) tidal radius:

$$r_t \simeq x_p \left[\frac{M_s}{M_g(3+e)} \right]^{1/3} \quad (20)$$

The above analytic forms for point masses are useful in explicitly showing that r_t has three limiting values at each position, $x_p < x < x_a$, of the satellite. From equation (19), we see that the prograde stripping radius ($\alpha = 1$) is smaller than the radial one ($\alpha = 0$) which is smaller than the retrograde one ($\alpha = -1$), as expected. However, in practise, point mass potentials are a poor approximation to galaxy mass distributions. In the following section, where we compare the theoretical tidal radii with N-body simulations, we solve equation (7) numerically for the same potentials as those used in the simulations. Using the point mass potentials instead can lead to errors in the tidal radii as large as a factor of two.

3 COMPARISON WITH NUMERICAL SIMULATIONS

We set up the initial conditions for the satellite by drawing the positions from an analytic density profile and the velocities from a numerically calculated distribution function. This process is described and tested in detail in a companion paper (Read et al. 2005). We note here that using distribution functions rather than the more familiar Maxwellian approximation (as in Hernquist 1993) for calculating particle velocities is much more accurate for simulations of tidal stripping (Kazantzidis et al. 2004).

We used a Plummer density profile for the satellite which is a self-gravitating, single component, spherical

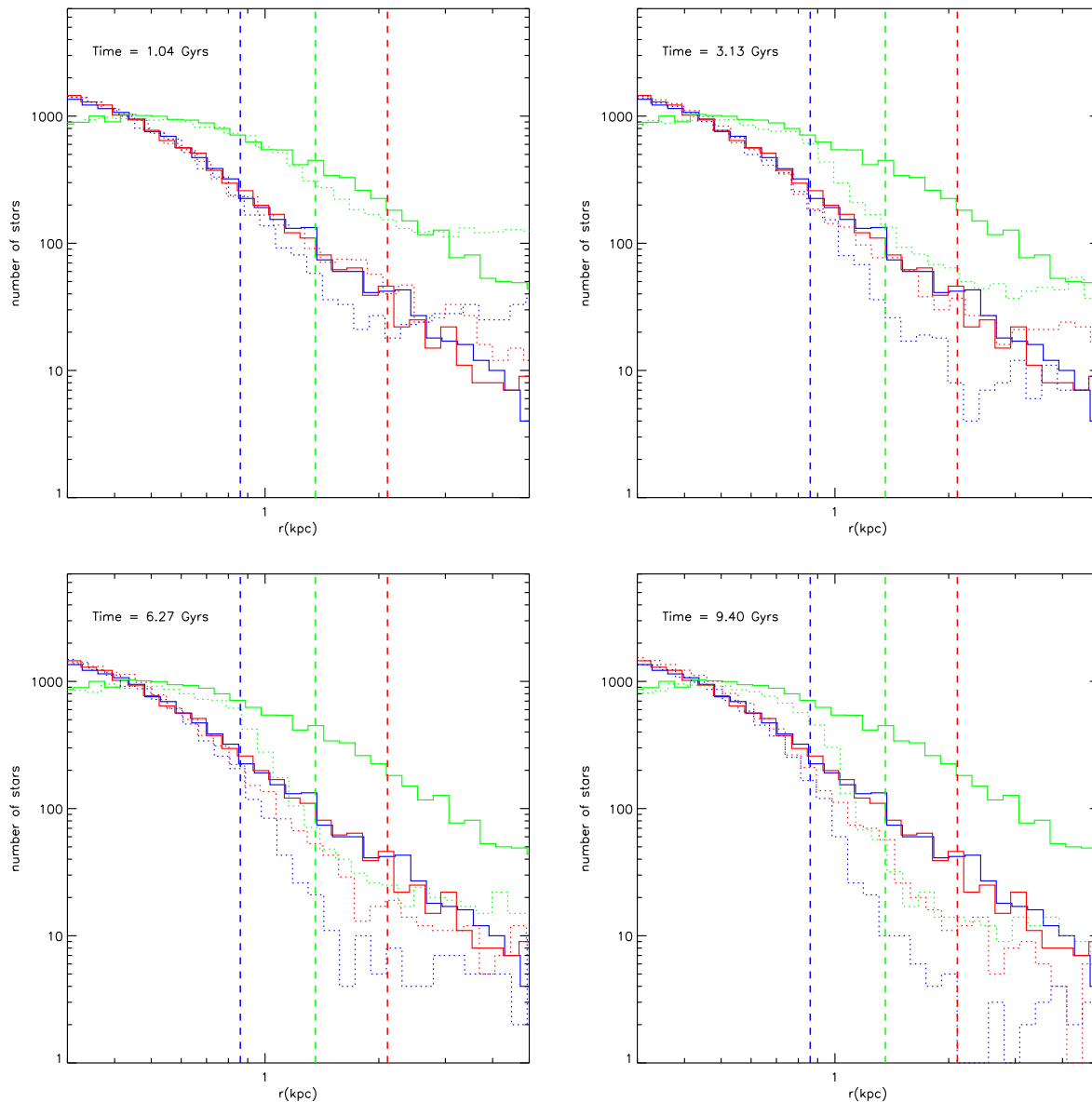


Figure 2. The tidal stripping of satellite stars as a function of the stellar orbits. Each panel shows a different time output as the satellite orbits around the host galaxy on a circular orbit at 80 kpc. The time is marked in the top left corner of each panel and increases down the page over 10 Gyrs. The blue, green and red lines show the radial distribution of stars which were initially on prograde, radial and retrograde orbits respectively. The solid lines show the initial distributions, while the dotted lines show the evolved profiles. The vertical dashed lines show the three analytic tidal radii calculated from equation 7: prograde (blue), radial (green) and retrograde (red).

galaxy comprising only stars. The Plummer profile is given by (Binney & Tremaine 1987):

$$\rho_{\text{plum}} = \frac{3M_s}{4\pi a_s^3} \frac{1}{\left(1 + \frac{r^2}{a_s^2}\right)^{5/2}} \quad (21)$$

where $M_s = 10^7 M_\odot$ and $a_s = 0.23 \text{ kpc}$ are the mass and scale length of the satellite respectively. The satellite velocity distribution was initially isotropic and when evolved in isolation was found to be extremely stable over a Hubble time. We used a simulation resolution of 10^5 particles for the satellite and a force softening of 10 parsecs; the simulations were found to be very well resolved - higher resolution test

runs (such as those presented in Read et al. 2005) produced converged results.

The initial conditions were evolved using a modified version of the GADGET N-body code (Springel et al. 2001) modified to permit a fixed potential to model the host galaxy. We used a host galaxy potential chosen to provide a good fit to the Milky Way (Law et al. 2005). We used a Miyamoto-Nagai potential for the Milky Way disc and bulge and a logarithmic potential for the Milky Way dark matter halo. These are given by respectively (see e.g. Binney & Tremaine 1987):

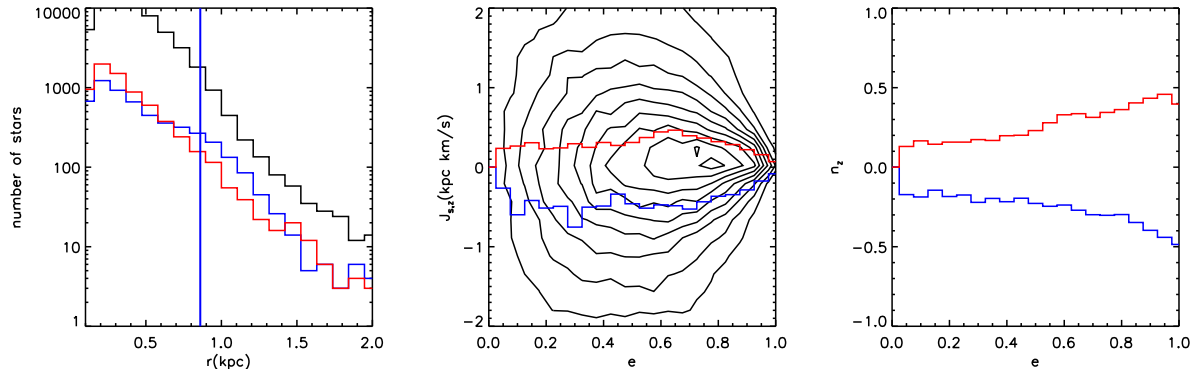


Figure 3. The evolution of star orbits within a satellite. The left panel shows, binned as a function of their initial radius, the number of stars which retain the original sense of their motion after 10 Gyrs (black line), the number converted from retrograde to prograde motion (blue line), and the number converted from prograde to retrograde (red line). The prograde stripping radius is also marked in blue. The middle panel shows a contour plot of the distribution of orbital eccentricity versus $J_{s,z}$ (the z component of the specific angular momentum) for the stars. The black contours show the initial distribution before stripping, the red and blue lines show the initial distribution for stars which have their orbits converted over 10 Gyrs from prograde to retrograde and retrograde to prograde respectively. The right panel shows the initial distribution of n_z and e for stars which have their orbits converted to prograde (blue line) and retrograde (red line) motion, where n_z is the mean z-component of the initial orbital pole of stars in a given eccentricity bin. Stars on a planar orbit initially have $n_z = \pm 1$, while those on a polar orbit have $n_z = 0$. Only stars which remain bound over 10 Gyrs have been included in these plots.

$$\Phi_{\text{mn}}(R, z) = \frac{-GM_d}{\sqrt{R^2 + (a + \sqrt{z^2 + b^2})^2}} \quad (22)$$

where $M = 5 \times 10^{10} M_\odot$ is the disc mass, $a = 4$ kpc is the disc scale length and $b = 0.5$ kpc is the disc scale height, and:

$$\Phi_{\text{log}}(r) = \frac{1}{2} v_0^2 \ln(R_c^2 + r^2) + \text{constant} \quad (23)$$

where $R_c = 4.1$ kpc is the halo scale length and $v_0 = 220$ km/s is the asymptotic value of the circular speed of test particles at large radii in the halo.

We held the satellite properties and the host galaxy properties fixed and varied only the orbit of the satellite about the host galaxy. We use a circular orbit at 80 kpc (section 3.1) and an eccentric orbit with apocentre 85 kpc and pericentre 23 kpc (section 3.3). These orbits are typical of Local Group dSph galaxies (see e.g. Piatek et al. 2002 and Piatek et al. 2005).

Finally, it is not trivial to mass and momentum centre the satellite when performing analysis of the numerical data. An incorrect mass centre can lead to spurious density and velocity features (Pontzen et al. 2005). We use the method of shrinking spheres to find the mass and momentum centre of the satellite (Power et al. 2003).

3.1 Circular satellite orbits

The first numerical test is a circular orbit of a satellite which experiences relatively weak tidal effects from the host galaxy. This is because the analytic formulae assume that the satellite potential remains constant. If a large fraction of the satellite’s mass is stripped away, this approximation starts to break down. In this case, the tidal radii should be recalculated at each time step iteratively as mass is removed, much as is done in semi-analytic simulations of tidal stripping (see e.g. Taffoni et al. 2003).

We wish to understand how a satellite star is affected by the host galaxy’s tidal field, as a function of the star’s orbit. In order to do this, we calculate the orbit of each star in the satellite initially. For a spherical system, the energy equation for an individual star can be simply rearranged to give (Binney & Tremaine 1987):

$$\dot{r}^2 = 2(E_s - V_s(r)) - J_s^2/r^2 \quad (24)$$

where \dot{r} is the radial velocity of the star with respect to the satellite’s centre of mass, E_s is the star specific energy, J_s is the star specific total angular momentum and $V_s(r)$ is the potential of the satellite.

At pericentre, r_p , and apocentre, r_a , $\dot{r} = 0$ and so we may calculate r_a and r_p for each satellite star by finding the roots of equation (24). We may then obtain the eccentricity of each star orbit, e , as defined in equation (15). In order to do this, we must know $V_s(r)$; and J_s and E_s for each star. The specific kinetic energy and angular momentum for each star may be simply computed from their phase space coordinates. For 10^5 star particles, the potential due to the self gravitating stellar distribution is prohibitively slow to compute via direct summation. To avoid this problem, we use a tree code to compute the potential (Dehnen 2000).

Ideally, we would like to compare pure circular and pure radial orbits with the analytic calculation in section 2. However, models built either with pure circular or pure radial orbits are unstable (see e.g. Binney & Tremaine 1987). We use instead an isotropic distribution of velocities which has the advantage that it is stable, but the disadvantage that very few stars are on either pure circular or pure radial orbits. To obtain good statistics, we define an orbit as being ‘circular’ if $e < 0.5$ and ‘radial’ if $e > 0.7$. The ‘circular’ orbits are then divided into prograde ($\mathbf{J}_s \cdot \mathbf{J} > 0$) and retrograde ($\mathbf{J}_s \cdot \mathbf{J} < 0$) orbits; where \mathbf{J}_s and \mathbf{J} are the star and satellite specific angular momentum vectors respectively. The radial orbit boundary ($e > 0.7$) is chosen such that there are as

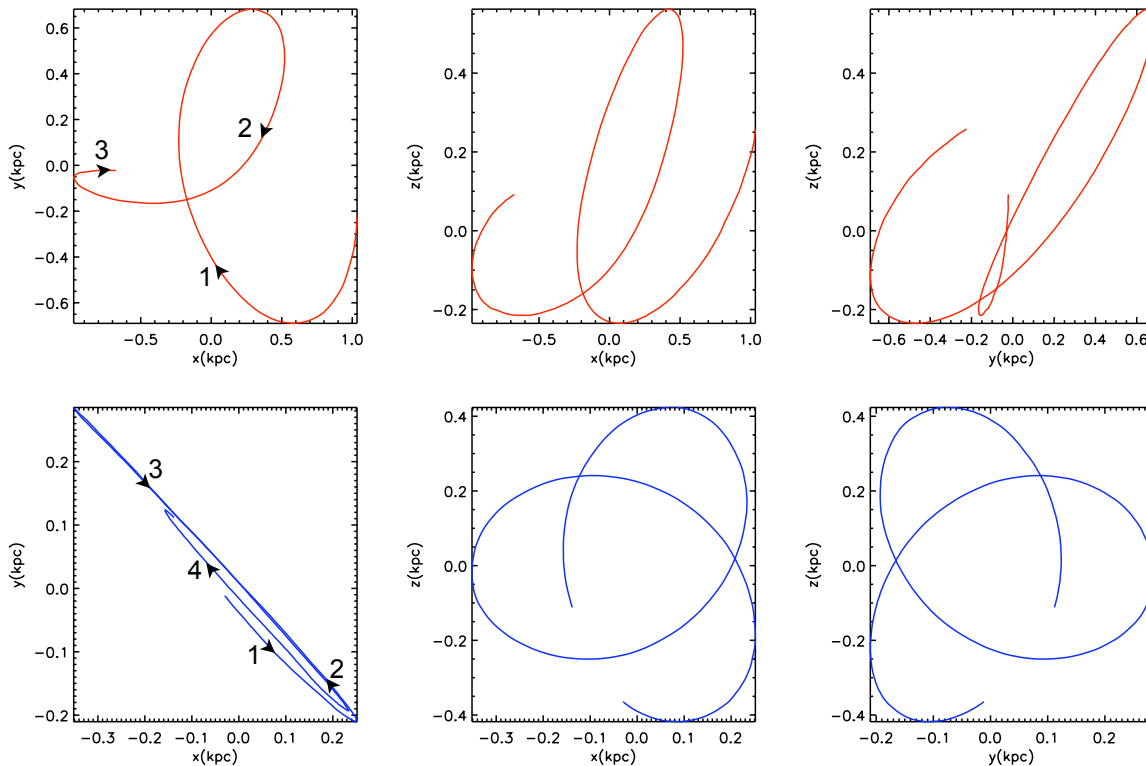


Figure 4. Space projections for two star orbits which were converted to retrograde motion (red line) and to prograde motion (blue line) over ~ 1 Gyr. Orbits were extracted from the simulation for a satellite on a circular orbit about the host galaxy (see section 3.1 and text for more details). The black arrows and numbers mark the direction of motion of the star in each case.

many stars on ‘radial’ orbits initially as there are on prograde or retrograde orbits.

Having divided up the initial stellar distribution in this way, we can track the evolution of prograde, radial and retrograde stars as the satellite orbits around the host galaxy. Figure 2 shows four snapshots in time over 10 Gyrs as the satellite orbits around the host galaxy.

From Figure 2, we can see that the analytic model works very well for the first Gyr. The dotted lines show that stripping occurs for each of the orbit-types only up to the analytic tidal radii. However, over longer time scales¹, all of the orbit types begin to become stripped into the prograde limit (blue dashed line). The natural question is then, what is causing this effect? Two obvious possibilities are that either the potential of the satellite has changed significantly, in which case the tidal radii should migrate inwards, or that the orbits of the stars have been altered by the tidal field of the host galaxy. By plotting the potential of the satellite as a function of time, it is easy to show that option one is not correct. As might be expected given the small number of stars which are actually stripped in this simulation, the

satellite potential remains almost constant over the whole simulation time of 10 Gyrs. Rather, the orbits of the stars are changing in the tidal field of the host galaxy. We discuss this further in the following section.

3.2 Tidal star-orbit transformations

Figure 3 shows the evolution of star orbits within the satellite over 4 Gyrs. Orbits which remain unchanged are shown by the black lines, those which have been converted to prograde (retrograde) motion are shown in blue (red). We include all stars which remain bound over 10 Gyrs in this plot and plot the *initial* properties of stars which have their orbits transformed. Unlike the previous section, we do not introduce any eccentricity cuts, but instead define stars as prograde or retrograde based on their value of $\underline{J}_s \cdot \underline{J}$.

In the left panel, we show the number of stars as a function of radius which have their orbits converted over 4 Gyrs. Orbital transformations only affect about 10% of the stars. Inside the prograde stripping radius, shown by the solid vertical blue line, it is more likely for stars to be converted to retrograde motion than to prograde. Outside the prograde stripping radius the opposite appears to be the case. In fact, prograde orbits always experience more efficient tidal transformations than retrograde orbits, in a statistical sense. This is for the same reason that prograde orbits are more

¹ The time for one circular orbit at 80kpc in the potential we use is ~ 2 Gyrs. Throughout this paper we refer to ‘short’ times as being $\lesssim 2$ Gyrs and ‘longer times’ as being $\gtrsim 2$ Gyrs.

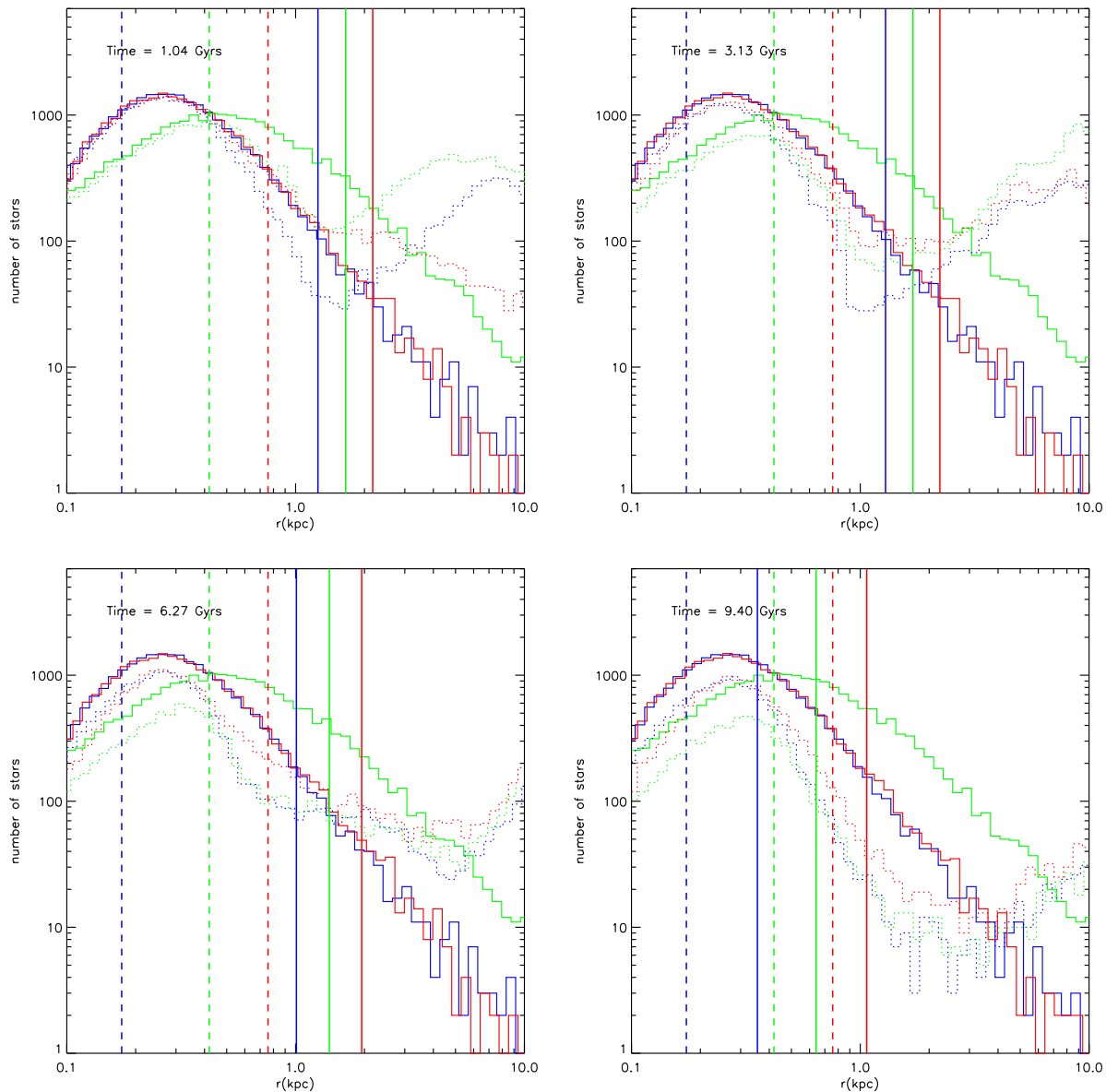


Figure 5. The tidal stripping of satellite stars as a function of the stellar orbits. Lines and panels are as in figure 2, but now the satellite is on a highly eccentric orbit with apocentre 85 kpc and pericentre 23 kpc. The vertical solid lines show the three tidal radii calculated at the current time; while the vertical dashed lines show the three tidal radii calculated at the pericentre (distance of closest approach) of the satellite’s orbit.

efficiently stripped by tides than retrograde orbits. What happens beyond the prograde stripping radius is that tidal stripping depletes the stars on prograde orbits. Stars are still being converted to retrograde and prograde motions in the same proportions as inside the prograde stripping radius, but now there are almost no stars left on prograde orbits - no stars left to be converted to retrograde motion; recall that in Figure 3, we do not include any unbound stars.

In the middle panel, we plot the initial distribution of e and $J_{s,z}$ for the stars (black contours), where $J_{s,z}$ is the z -component of the star specific angular momentum and e is the eccentricity. Overlaid is the binned distribution of initial e and mean $J_{s,z}$ for those stars which have their orbits converted to prograde (blue line) and retrograde (red line)

motion. This plot shows us that such stars are preferentially those on high e and low $J_{s,z}$ orbits. This is as might be expected: stars on highly eccentric orbits sample radii far away from the satellite centre of mass and so are more affected by tides, while stars with low $J_{s,z}$ do not need to alter their angular momentum greatly to move onto prograde rather than retrograde orbits (or visa-versa).

In the right panel, we plot the initial distribution of n_z and e for stars which have their orbits converted to prograde (blue line) and retrograde (red line) motion, where n_z is the mean z -component of the initial orbital pole of stars in a given eccentricity bin. This plot shows us that stars which have their orbits converted are preferentially on polar ($n_z = 0$) rather than planar ($n_z = \pm 1$) orbits. Orbits which are

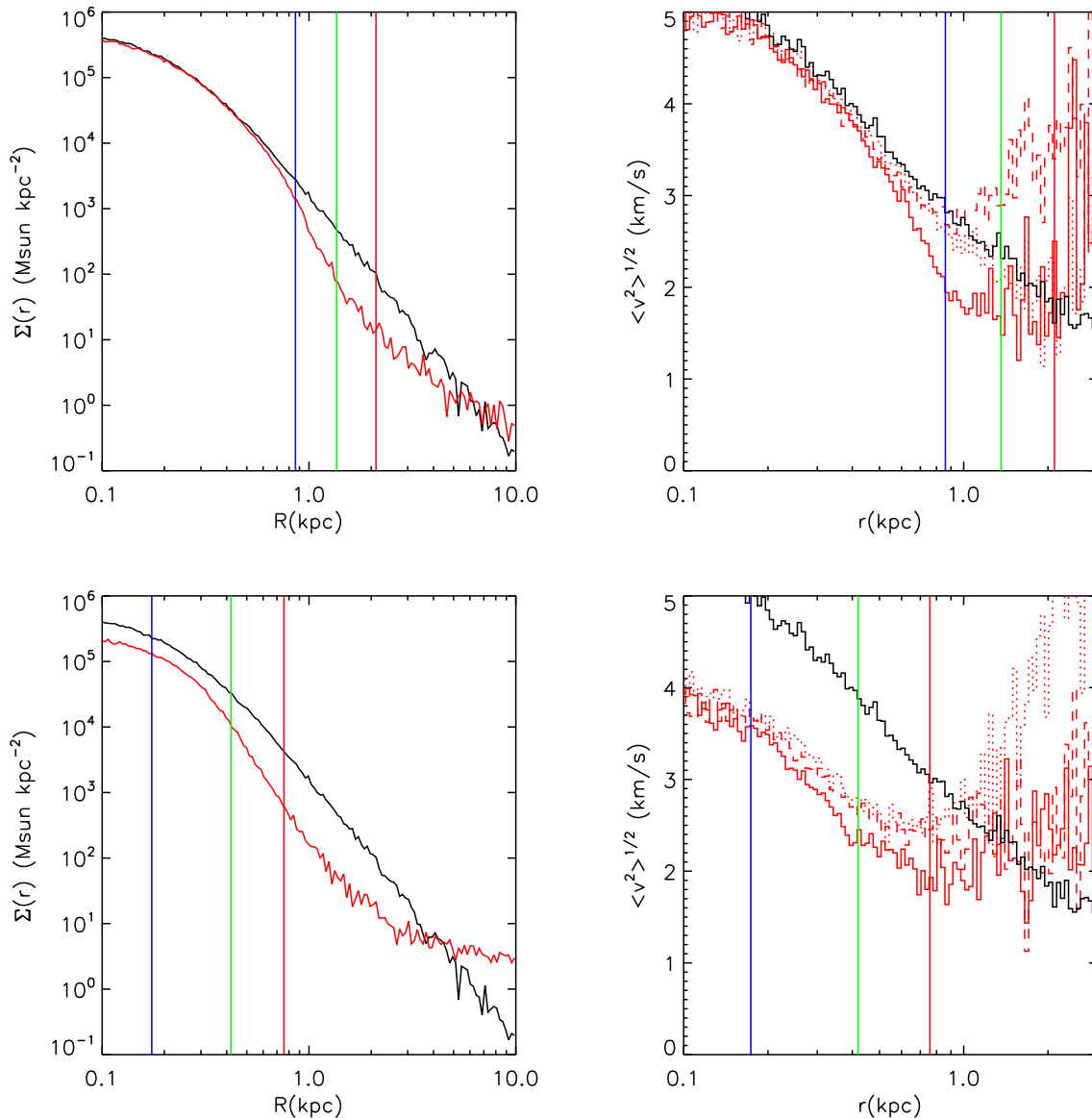


Figure 6. The projected surface brightness distribution (left) and velocity dispersion (right) for a satellite on a circular orbit (top panels and see section 3.1) and an eccentric orbit (bottom panels and see section 3.3). The black lines show the initial profiles while the red lines show the profiles after ~ 10 Gyrs. The solid vertical red, green and blue lines show the three analytic tidal radii from equation 7. In the plot of the velocity dispersions, the solid red line shows the radial velocity dispersion while the dotted and dashed lines show the θ and ϕ components.

planar and become transformed have preferentially higher eccentricities. Orbital transformations are easiest for those stars with the smallest $J_{s,z}$ component.

In Figure 4, we plot two star orbits which were converted to retrograde motion (red line) and to prograde motion (blue line) over ~ 1 Gyr. These illustrate the mechanisms which drive such orbital transformations. In the first mechanism, (top three space projections) tidal forces act along the direction of motion of the star. In this case, an initially prograde orbit loses its tangential velocity and is converted to a radial orbit. After further deceleration, the final orbit is only very slightly retrograde and appears nearly radial in the plot. In the second mechanism, the star is on a

more polar orbit. Tidal forces acting perpendicular to star's orbit plane tilt the orbit about the z-axis, causing a flip from retrograde to prograde motion. These two mechanisms are quite different in that, in the first, stars are transformed through radial orbits, while in the second, a star may remain on a relatively circular orbit throughout the transformation. Since only a few stars will be initially on very polar orbits, it is the first mechanism which is the dominant one. This is an important point which we discuss further in section 3.4.

The result of these orbital transformations is that the three tidal radii of section 2, over long times, converge on the prograde stripping radius. This is because any star beyond the prograde stripping radius which has its orbit trans-

formed to prograde is rapidly stripped. Over long times it becomes increasingly likely that low angular momentum, high eccentricity, stars - both prograde and retrograde - will for a short time be pushed onto a prograde orbit, at which point they will be carried away by tides.

3.3 General satellite orbits

In this section, we consider the more complicated case of a satellite on a highly eccentric orbit. We use an orbit with apocentre 85 kpc and pericentre 23 kpc. Figure 5 shows four snapshots in time over 10 Gyrs.

As discussed in section 2, the three limiting tidal radii for prograde (blue dashed line), retrograde (red dashed line) and radial (green dashed line) are functions of time. This is why the solid lines are in different places in the panels of Figure 5. The dashed vertical lines in Figure 5 show the values of the three tidal radii at the pericentric distance of the satellite; these do not vary with time.

Notice that there are now two points at which the satellite stars show a tidal ‘break radius’. One is at the current tidal radius, the other is close to the pericentric tidal radius. Similar results for the surface brightness distributions have been observed by other authors (see e.g. Johnston et al. 2002). Each of these break radii are split into three further limiting tidal radii as a function of the star orbits.

Over long timescales ($\gtrsim 8$ Gyrs), the break radius which lies at the current tidal radius of the satellite’s orbit disappears. This is because, after the initial distribution has been stripped of all stars beyond their tidal radii, further stripping can only occur as stars heated by the tidal field of the host galaxy migrate outwards. This effect is much smaller and produces only a tiny perturbation on the surface brightness profile which, at these late times, now appears much smoother.

Notice that over a Hubble time, the central density of all orbits lowers in its normalisation, even in the very centre of the satellite. This is not due to tidal stripping, but rather to a different physical effect which occurs only for highly eccentric orbits, or for orbits which cause the satellite to pass through the plane of the disc - namely tidal shocking (see e.g. Gnedin & Ostriker 1997, Gnedin et al. 1999 and Gnedin et al. 1999). These tidal shocks can (and in this case do) become more important than stripping in the very centre of the satellite. We discuss the effects of tidal shocks in more detail in a companion paper, (Read et al. 2005).

As for the circular orbit case, orbital transformations drive all star orbits eventually towards the prograde limit at pericentre (blue solid vertical line). However it is difficult to ascertain whether the prograde limit is ever actually reached in practice for general satellite orbits because of the action of tidal shocks.

3.4 Implications of the new tidal radii

A natural question relates to the observability of the three tidal radii in the projected surface brightness profile and velocity dispersion of the stars. These are shown in Figure 6. Notice that if only surface brightness information were available, the tidal radius determined purely from ‘features’ in the light profile would be erroneous. For the case of a

satellite on a circular orbit (top panels), the surface brightness profile is depleted at the prograde stripping radius (blue vertical line) and breaks at the retrograde stripping radius (red vertical line). For a more general satellite orbit (bottom panels) there are no observable features in the light profile at any of the analytic tidal radii. This is because tidal shocking washes out such information (notice that such tidal shocks also lower the central surface brightness as the satellite becomes puffed up). However, if the radial and tangential velocity dispersions are known then the tidal radii may be much better determined. Notice that for both the satellite on the circular orbit and the more general orbit, tangential velocity anisotropy appears at the prograde stripping radius. This is because, as discussed in section 3.2, stars on radial or near radial orbits are, over long times, pushed momentarily onto prograde orbits, at which point they are stripped away. Thus even at the prograde stripping radius, there is a depletion of radial orbits with respect to retrograde orbits and this leads to the onset of tangential anisotropy. Such anisotropies increase outwards as stars moving on radial orbits become more easily stripped at the radial stripping radius. The presence of tangential anisotropy provides a much more robust signature of the true tidal radius than can be measured from the light profile alone.

4 CONCLUSIONS

We have presented an improved analytic calculation for the tidal radius of satellites and tested our results against N-body simulations.

The tidal radius in general depends upon four factors: the potential of the host galaxy, the potential of the satellite, the orbit of the satellite and *the orbit of the star within the satellite*. We demonstrated that this last point is critical and suggest using *three tidal radii* to cover the extrema range of orbits of stars within the satellite. In this way we showed explicitly that prograde star orbits will be more easily stripped than radial orbits; while radial orbits are more easily stripped than retrograde ones. This result has previously been established by several authors numerically. We showed further that, in general, the tidal radius *does not depend only on the enclosed mean density of the satellite*. While for stars on pure radial orbits it is reasonable to approximate the tidal radius as being that where the density of the satellite matches that of the host galaxy, for prograde and retrograde star orbits, the tidal radius also depends on the *mass distribution* of the satellite galaxy.

Over short times ($\lesssim 1 - 2$ Gyrs ~ 1 satellite orbit), we find excellent agreement between our analytic and numerical models. Over longer times, star orbits within the satellite are transformed by the tidal field of the host galaxy. In a Hubble time, this causes a convergence of the three limiting tidal radii towards the prograde stripping radius.

Satellites which have been tidally stripped will show tangential velocity anisotropy near their tidal radii, with a depletion of both prograde and radial orbits relative to the retrograde orbits. This must be true irrespective of the initial conditions. These results naturally explain the numerical observations dating back to Toomre & Toomre (1972) and Keenan & Innanen (1975) which found exactly these

velocity anisotropies in their simulations of galaxy-satellite interactions.

In the future, with improved kinematic data for nearby satellites from GAIA or SIM, it may be possible to search for tangential velocity anisotropies as a ‘smoking gun’ from tidal stripping, and thereby much better determine the tidal radii of nearby galaxies and star clusters. This would represent a significant improvement on current methods which have historically found ‘tidal radii’ from features in the surface brightness profiles alone.

REFERENCES

- Baumgardt H., Makino J., 2003, MNRAS, 340, 227
 Binney J., Tremaine S., 1987, Galactic dynamics. Princeton, NJ, Princeton University Press, 1987, 747 p.
 Dehnen W., 2000, ApJ, 536, L39
 Giersz M., Heggie D. C., 1997, MNRAS, 286, 709
 Gnedin O. Y., Hernquist L., Ostriker J. P., 1999, ApJ, 514, 109
 Gnedin O. Y., Lee H. M., Ostriker J. P., 1999, ApJ, 522, 935
 Gnedin O. Y., Ostriker J. P., 1997, ApJ, 474, 223
 Hernquist L., 1993, ApJS, 86, 389
 Johnston K. V., Choi P. I., Guhathakurta P., 2002, AJ, 124, 127
 Kazantzidis S., Magorrian J., Moore B., 2004, ApJ, 601, 37
 Keenan D. W., Innanen K. A., 1975, AJ, 80, 290
 King I., 1962, AJ, 67, 471
 Kravtsov A. V., Gnedin O. Y., Klypin A. A., 2004, ApJ, 609, 482
 Law D. R., Johnston K. V., Majewski S. R., 2005, ApJ, 619, 807
 Mateo M. L., 1998, ARA&A, 36, 435
 Moore B., Ghigna S., Governato F., Lake G., Quinn T., Stadel J., Tozzi P., 1999, ApJ, 524, L19
 Piatek S., et al., 2005
 Piatek S., Pryor C., Olszewski E. W., Harris H. C., Mateo M., Minniti D., Monet D. G., Morrison H., Tinney C. G., 2002, AJ, 124, 3198
 Pontzen A., Read J. I., Ricotti M., Viel M., 2005, . In preparation.
 Power C., Navarro J. F., Jenkins A., Frenk C. S., White S. D. M., Springel V., Stadel J., Quinn T., 2003, MNRAS, 338, 14
 Read J. I., Wilkinson M. I., Evans N. W., Gilmore G., Kleya J. T., 2005, . In preparation.
 Springel V., Yoshida N., White S. D. M., 2001, New Astronomy, 6, 79
 Taffoni G., Mayer L., Colpi M., Governato F., 2003, MNRAS, 341, 434
 Takahashi K., Lee H. M., Inagaki S., 1997, MNRAS, 292, 331
 Toomre A., Toomre J., 1972, ApJ, 178, 623
 von Hoerner S., 1957, ApJ, 125, 451